Available online at www.sciencedirect.com
ScienceDirect
Journal of Sound and Vibration 321 (2009) 762–785
JOURNAL OF SOUND AND VIBRATION
www.elsevier.com/locate/jsvi

Sensitivity analysis of blast loading parameters and their trends as uncertainty increases

E. Borenstein*, H. Benaroya

Rutgers University, Piscataway, NJ, USA

Received 2 April 2008; received in revised form 11 October 2008; accepted 13 October 2008
Handling Editor: S. Bolton
Available online 3 December 2008

Abstract

A sensitivity analysis of blast loading parameters is performed to determine which of the parameters' uncertainties have the greatest effect on the maximum deflection of a clamped aluminum plate subjected to a blast load. A numerical simulation using the Monte Carlo method is used to obtain the ensemble averages of the probabilistic runs, with random variables given uniform distributions. The first loading model has an instantaneous rise with an exponential decay, represented by the modified Friedlander equation. The second loading model has a linear rise with an exponential decay. Both of these models are simulated with three different scaled blast loads, giving a total of six different cases. In addition, the deflection trends due to increases in loading uncertainties are quantified. Probability density functions for the maximum deflections are estimated. The probabilistic results and trends are also explained using deterministic methods. It is concluded that response is most sensitive to loading duration time.

1. Introduction

Due to the rise of terrorism, the commercial aviation industry has a great need to understand the effects of an on-board explosion in order to improve the designs of luggage containers and aircraft. It is also important to locate the areas of the aircraft that are most vulnerable to an explosive load. Knowing these locations and the amount of loading needed to cause critical failures provides a baseline for explosive detection technologies. In order to obtain these data, many costly and time consuming experiments are being performed. As an alternative, finite element codes can help analyze the response of structures to given loading. However, these codes can be rather time consuming. Therefore, an accurate simplified model of the response of an aircraft structure subjected to a blast load would be of great use to the aviation industry.

Aside from a simplified response model, an accurate loading model is needed. Many experiments have been performed to analyze different types of explosives. During these complex and costly blast experiments, a variety of sensors and devices are used to capture the loading on the structure. The positioning of the sensors

*Corresponding author. Tel.: +1 732 445 1401.
E-mail address: elanb@rci.rutgers.edu (E. Borenstein).

0022-460X/$ - see front matter
doi:10.1016/j.jsv.2008.10.017

and the accuracy of the devices generally lead to uncertainty of loading measurements, exclusive of the random characterization associated with the explosives.

In this paper, sensitivity analyses of blast loading parameters are performed to determine which blast model parameter uncertainties has the greatest effects on the maximum deflection of a clamped aluminum plate. In addition, we quantify how the deflection trends as a result of parameter uncertainties. Such results can be used to determine beforehand which experimental parameters must be measured most precisely in order to capture the fundamental behavior of the blast loading and structural response. This will help experimentalists in deciding which instrumentation and setup will collect the best set of data. Also the number of dangerous, expensive and time consuming experiments that are needed can be reduced.

For instance, consider an experimentalist who would like to obtain an accurate pressure profile of a particular explosion in order to study how that size explosion affects a structure. The experimentalist may want to perform numerous, identical blast experiments and use the average of all the experiments as the final, ''accurate'' pressure profile. During the experiment there are a number of instruments and equipment that need to be designed and/or chosen. Even the placement of the instrumentation has a key role in obtaining proper data. The experimentalist sets up the experiment in a way to obtain the most accurate result. However, what if the experimentalist had to choose between measuring a certain parameter more precisely verses another parameter? For example, one can choose an instrument that has a more precise pressure reading than some other instrument, but does not take the readings as often. This instrument will have less uncertainty to the pressure reading, however, it will increase the uncertainties of duration time and rise time. This sensitivity analysis will help determine which of the parameters should be more accurately measured in order to reduce the amount of uncertainty in the measurements.

We use approximate analytical models to numerically model a clamped, thin aluminum plate, representative of a fuselage section, subjected to a simplified blast load and calculate the maximum transverse deflection occurring at the plate's center. We then randomize the various loading parameters to see how their uncertainties affect the plate's maximum deflection. We define sensitivity as the difference between maximum deflections of the randomized model and the deterministic model.

2. Literature review on blast loading

There have been a few books dedicated to explosive loading. Kinney and Graham wrote the comprehensive book, ''Explosive Shocks in Air'' [1], which explains many different aspects and characteristics of explosive loads. Another extensive book on blast loading is ''Explosions in Air'' [2] by Baker. Aside from an overview of explosive loading, this book includes a compilation of experimental equipment and data, as well as some computational methods. A much cited book that deals with explosive loads is ''Explosion Hazards and Evaluation'' [3] by Baker, Cox, Westine, Kulesz and Strehlow. This book has an extensive compilation of experimental work.

In addition to books, there have been a number of review papers. Florek and Benaroya [4] provide an extensive review on pulse-loading effects on the deflection of structures. In addition, they summarize efforts that try to reduce or eliminate these pulse shape effects, which can be done for many rigid-plastic geometries under a uniform load. A detailed description is provided of research on pressure-impulse isodamage curves along with some background on the sensitivity of the structural response due to various loading models.

Beshara [5] provides an extensive review of the analysis of unconfined blast loading due to different sources for above ground rigid structures. He discusses the use of TNT equivalency and blast scaling laws, as well as the differences between overpressure, reflective pressure and dynamic pressure. Reviewing the available unclassified literature, Beshara concluded that ''precise loading information is hard to obtain and may be not justified because of the many uncertainties involved in the interaction process between the blast wave and the structure and the ideal gas assumption in the derivation of relevant relations …''. He adds that the way a blast load affects the response of a structure does not only depend upon the magnitude of the load, but also on its duration, rise time and general shape. The implication is that a good blast loading model is important, but its effects are very sensitive to small changes in these characteristics.

Chock and Kapania [6] review blast scaling, particularly the Hopkinson–Cranz and the Sachs blast scaling. They then compare two methods for calculating the loading profiles of explosive blasts in air. One method is

from Baker [2], which uses Sachs scaling and the other method is from Kingery and Bulmash [7], which uses Hopkinson–Cranz scaling. They concluded that the reflected peak pressures are of a similar order of magnitude but there is a difference in the specific impulses delivered to the target. For the case given in Chock and Kapania, Baker's method has a much lower impulse and an earlier arrival time than Kingery and Bulmash's method. They mention that this could be attributed to the difference in duration time, as well as a change in the way that the decay values are determined. They were unable to determine which of the two methods is more precise because both methods are based on experimental data, with few or no repeated tests.

Esparza [8] did experimental work on TNT and other high explosives at small scaled distances. He states that using a single equivalent weight ratio may not be appropriate to characterize an explosive load, especially at small scaled distances because there is insufficient experimental verification. In regards to TNT equivalency, he mentions that an equivalent system with only one blast parameter may not be accurate because TNT equivalence can be significantly different depending on the scaled distance of the explosive, even with the same type of explosive. Esparza did a study and comparison to published data [7] on the peak overpressure, arrival time, impulse and positive duration of the blast loads in his experiments. He noticed that the TNT equivalency for some of the parameters can be significantly different than one based on heat of detonation. In addition, for small scaled distances, the impulse and positive duration parameters are not as well defined as the pressure and arrival time parameters.

Gatto and Krznaric [9] performed experiments on explosive loads in aircraft luggage containers. They measured the pressure profiles on the container panels due to explosions with different amounts of luggage inside. They noticed that additional luggage reduces the pressure on the container significantly. In addition, the location of the bag with the explosives has a significant effect on the loading the container experiences.

Simmons and Schleyer [10] did experimental and finite element analysis of the response and failure modes of stiffened, aluminum alloy panels with conventional riveting and laser welding. They used a pressure chamber that theoretically gives a triangular pressure pulse on the test structure. They concluded that riveted joints have greater energy absorbing capacity than laser-welded joints. In addition, the joints' energy absorption is sensitive to the load rate.

Gantes and Pnevmatikos [11] proposed a response spectra based on a blast pressure profile with an exponential distribution and then compared it to one with a triangular distribution. In their work, they used a technique recommended by the US Department of the Army TM5-1300 [12] which is based upon substituting the structural element by a stiffness equivalent, single degree-of-freedom system, and using elastic–plastic response spectra to predict the maximum response of the system. They observed that a triangular distributed load can sometimes be slightly unconservative compared to the exponential decay load, particularly for flexible structural systems. In addition, the triangular distributed load can be significantly overconservative compared to the exponential decay load for stiffer structures. They state that since exponential loading decreases faster than a triangular one, the differences between the two are influenced more in elastic–plastic situations than in purely elastic ones. In addition, they provide ranges for certain parameters in which the differences in blast loading profiles play significant roles in the responses. Referring to Watson [13], the response depends on synchronization with the rebound of the structure, which means that a good knowledge of blast load time and space variation are critical to obtain the correct response. In addition, Watson says that the influence of damping on these systems can be neglected because the peak response of the system occurs within the first few cycles. This allows for a much simpler response equation.

Bogosian et al. [14] used experimental data to compare a variety of simplified models, including BlastX, ConWep and SHOCK, to measure the inherent uncertainty in these blast model codes. The data they analyze are restricted to a Hopkinson–Cranz scaled range of 3–100 $\mathrm{ft/lb^{(1/3)}}$. Although their final test database was comprised 303 individual gage records, they noted that not all were of sufficient duration and/or quality to be useful. Some have bad peak pressure readings and therefore could not produce reliable impulses. In addition, the test data were comprised a wide range of configurations from cylindrical to spherical to hemispherical charges. Different types of explosives were also used, including TNT, C-4 and ANFO, which were converted into their TNT equivalent load before computing the scaling factors. This shows how difficult it is to obtain a complete and accurate set of experimental work to analyze and understand the entire spectrum of blast loadings. However, Bogosian et al. were able to show that, of the tools they analyzed, ConWep best represented the test data in an overall sense. They also show that BlastX provides values that are close to the

data set, but SHOCK significantly underpredicts reflected positive pressure and overpredicts reflected positive impulse. By calculating the standard deviations of the test data, they noticed that their two-sigma values range from $\frac{1}{3}$ to $\frac{2}{3}$ in magnitude, which indicates a very wide range of uncertainty.

Trying to obtain a simplified, yet accurate model for blast loadings is a subject for continued research. These publications, which are mainly focused on loading models, show that there is a great amount of uncertainty involved when dealing with blast load modeling. In addition, many of the publications show that the response of a structure is very sensitive to the loading model.

3. Elastic response model

For the elastic region, the response model used here is outlined in Florek and Benaroya [15], which is developed from the works of Bauer [16], Singh and Singh [17] and Florek [18]. The two fundamental equations that govern the nonlinear vibration of plates subjected to a time dependent pressure load are given by

$$\nabla^4 F = \left\{ \left(\frac{\partial^2 w}{\partial x \partial y} \right)^2 - \frac{\partial^2 w}{\partial x^2} \frac{\partial^2 w}{\partial y^2} \right\} \tag{1}$$

and

$$\frac{Eh^3}{12(1-\nu^2)} \nabla^4 w + \rho h \ddot{w} = P(x,y,t) + h \left\{ \frac{\partial^2 F}{\partial y^2} \frac{\partial^2 w}{\partial x^2} + \frac{\partial^2 F}{\partial x^2} \frac{\partial^2 w}{\partial y^2} - 2 \frac{\partial^2 F}{\partial x \partial y} \frac{\partial^2 w}{\partial x \partial y} \right\}, \tag{2}$$

where w is the transverse deflection of the plate, ρ the mass density of the plate, E the elastic modulus, υ Poisson's ratio, h the plate thickness, P the loading pressure and $\nabla^4 \equiv \partial^4/\partial x^4 + 2\partial^4/\partial x^2 \partial y^2 + \partial^4/\partial y^4$. F is the Airy stress function which is related to the stresses by $\sigma_x = \partial^2 F/\partial y^2$, $\sigma_y = \partial^2 F/\partial x^2$ and $\sigma_{xy} = -\partial^2 F/\partial x \partial y$, where σ_x, σ_y and σ_{xy} are membrane stresses. When using Eqs. (1) and (2), the effects of longitudinal and rotary inertia forces are neglected.

The transverse deflection of the clamped plate is assumed to be of the form

$$w(x,y,t) = hf(t) \cos^2 \frac{\pi x}{a} \cos^2 \frac{\pi y}{b}, \tag{3}$$

where a and b are the length and width of the plate, respectively. The origin of the coordinate system $x\ y\ z$ is located at the center of the plate, as shown in Fig. 1. The maximum transverse deflection is equal to $hf(t)$ at any time t. In order to separate the space and time variables, the Airy stress function is assumed to be of the form

$$F(x,y,t) = F^*(x,y) f^2(t). \tag{4}$$

Substituting Eqs. (3) and (4) into Eq. (1) yields

$$\begin{aligned} \nabla^4 F(x,y,t) = & -\frac{Eh^2}{2a^2 b^2} f^2(t) \left(\cos \frac{2\pi x}{a} + \cos \frac{2\pi y}{b} + 2 \cos \frac{2\pi x}{a} \cos \frac{2\pi y}{b} + \cos \frac{4\pi x}{a} + \cos \frac{4\pi y}{b} \right. \\ & \left. + \cos \frac{2\pi x}{a} \cos \frac{4\pi y}{b} + \cos \frac{4\pi x}{a} \cos \frac{2\pi y}{b} \right). \end{aligned} \tag{5}$$

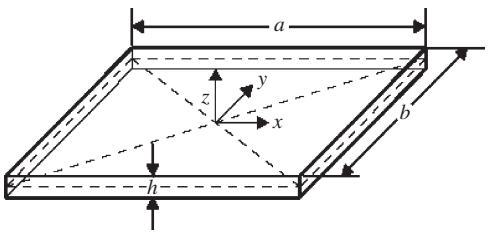

Fig. 1. Plate geometry and coordinate system.

Using Eq. (5), we are able to solve for the Airy stress function, $F(x,y,t)$, by assuming it is of the form

$$F(x,y,t) = f^2(t)\left(C_1x^2 + C_2y^2 + C_3\cos\frac{2\pi x}{a} + C_4\cos\frac{2\pi y}{b} + C_5\cos\frac{2\pi x}{a}\cos\frac{2\pi y}{b} + C_6\cos\frac{4\pi x}{a} + C_7\cos\frac{4\pi y}{b} + C_8\cos\frac{2\pi x}{a}\cos\frac{4\pi y}{b} + C_9\cos\frac{4\pi x}{a}\cos\frac{2\pi y}{b}\right), \tag{6}$$

where the C_n terms are constants. The midplane displacements, u and v, in the x and y directions, are, respectively,

$$u = \int_0^x \left\{ \frac{1}{E}\left(\frac{\partial^2 F}{\partial y^2} - \nu\frac{\partial^2 F}{\partial x^2}\right) - \frac{1}{2}\left(\frac{\partial w}{\partial x}\right)^2 \right\} \mathrm{d}x \tag{7}$$

and

$$v = \int_0^y \left\{ \frac{1}{E}\left(\frac{\partial^2 F}{\partial x^2} - \nu\frac{\partial^2 F}{\partial y^2}\right) - \frac{1}{2}\left(\frac{\partial w}{\partial y}\right)^2 \right\} \mathrm{d}y. \tag{8}$$

The boundary conditions for immovable plate edges are

$$u = 0 \quad \text{and} \quad \frac{\partial^2 F}{\partial x \partial y} = 0 \quad \text{at } x = \pm\frac{a}{2} \tag{9}$$

and

$$v = 0 \quad \text{and} \quad \frac{\partial^2 F}{\partial x \partial y} = 0 \quad \text{at } y = \pm\frac{b}{2}. \tag{10}$$

We then substitute the Airy stress function and Eq. (3) into Eq. (2). The Airy stress function and Eq. (3) satisfy the boundary conditions as well as Eq. (1). However, as mentioned in Bauer [16], they may not exactly satisfy Eq. (2). The Galerkin method is used with the assumed mode shape for the clamped plate to set up the residue equation

$$\int_0^{b/2}\int_0^{a/2} R\cos^2\frac{\pi x}{a}\cos^2\frac{\pi y}{b}\,\mathrm{d}x\,\mathrm{d}y = 0, \tag{11}$$

which results in the nonlinear elastic equation of motion for a clamped plate [18],

$$\rho h^2\ddot{f}(t) + \frac{4Eh^4\pi^4}{27a^4(1-\upsilon^2)}\left(3 + 2\frac{a^2}{b^2} + 3\frac{a^4}{b^4}\right)f(t) + \frac{Eh^4\pi^4}{a^4}\left\{\frac{1 + 2\upsilon a^2/b^2 + a^4/b^4}{8(1-\upsilon^2)} + \left[\frac{17}{144} + \frac{a^4}{9b^4}\left(\frac{17}{16} + \frac{2}{(1+a^2/b^2)^2} + \frac{1/2}{(1+4a^2/b^2)^2} + \frac{1/2}{(4+a^2/b^2)^2}\right)\right]\right\} f^3(t) = \frac{16}{9}P(t). \tag{12}$$

P is the uniform loading pressure. Numerically solving Eq. (12) for $f(t)$ yields the deflection at the center of the plate, $hf(t)$, until the plate yields.

3.1. Yield condition

In order to determine when the response is no longer in the elastic region governed by Eq. (12), a von Mises yield condition is initially used. As outlined in Florek and Benaroya [15], the von Mises condition given by Massonnet [19] is

$$Y_c \equiv \frac{M_x^2 + M_y^2 - M_xM_y + 3M_{xy}^2}{M_0^2} + \frac{N_x^2 + N_y^2 - N_xN_y + 3N_{xy}^2}{N_0^2} - 1 = 0, \tag{13}$$

where M_k represents the elastic bending moments per unit length and N_k represents the elastic membrane forces per unit length, in the k direction. M_0 and N_0 are the plastic bending moment per unit length and the

plastic membrane force per unit length, respectively. Lee [20] gives these parameters as

$$M_x = \frac{-Eh^3}{12(1-\nu^2)}\left(\frac{\partial^2 w}{\partial x^2} + \upsilon\frac{\partial^2 w}{\partial y^2}\right),$$

$$M_y = \frac{-Eh^3}{12(1-\nu^2)}\left(\frac{\partial^2 w}{\partial y^2} + \upsilon\frac{\partial^2 w}{\partial x^2}\right),$$

$$M_{xy} = \frac{-Eh^3}{12(1+\nu)}\frac{\partial^2 w}{\partial x \partial y},$$

$$M_0 = \frac{\sigma_0 h^2}{4},$$

$$N_x = h\frac{\partial^2 F}{\partial y^2},$$

$$N_y = h\frac{\partial^2 F}{\partial x^2},$$

$$N_{xy} = -h\frac{\partial^2 F}{\partial x \partial y},$$

$$N_0 = \sigma_0 h, \tag{14}$$

where σ_0 is the dynamic yield stress of the plate material. The dynamic yield stress is the stress level at which point the material begins to flow.

Using the Airy stress function, Eqs. (3), (13) and (14), we obtain the von Mises yield criterion for a clamped plate,

$$Y_c = \frac{E^2 h^4 \pi^4}{a^2 \sigma_0^2}\left[\frac{L_n^*}{1024} f^4(t) + \frac{4L_m}{9b^4(1-\upsilon^2)^2} f^2(t)\right] - 1, \tag{15}$$

where

$$L_m = (a^4 + b^4)(\upsilon^2 - \upsilon + 1) - a^2 b^2(\upsilon^2 - 4\upsilon + 1),$$

$$L_n^* = A^2 + AB + B^2,$$

$$A = \frac{3}{(1-\upsilon^2)}\left(1 + \upsilon\frac{a^2}{b^2}\right) + 5 + \frac{4a^4}{b^4}\left[\frac{2}{(1+a^2/b^2)^2} + \frac{4}{(1+4a^2/b^2)^2} + \frac{1}{(4+a^2/b^2)^2}\right],$$

$$B = \frac{3}{(1-\upsilon^2)}\left(\upsilon + \frac{a^2}{b^2}\right) + \frac{5a^2}{b^2} + \frac{4a^2}{b^2}\left[\frac{2}{(1+a^2/b^2)^2} + \frac{1}{(1+4a^2/b^2)^2} + \frac{4}{(4+a^2/b^2)^2}\right].$$

Once $Y_c > 0$, the plate begins to yield. As per Massonnet [19], it is assumed that the elastic–plastic interactions in a membrane are negligible and, after yielding begins, the response enters the purely plastic region. In the plastic region a new model is needed to represent the response of the plate. However, once the deflection of the plate begins to decrease, it does so elastically and is then modeled using the elastic model. At this point, the deflection at yielding becomes the maximum displacement the plate has previously reached. Therefore, once the plate deflection surpasses the previous maximum deflection, the plastic model is used until the deflection begins to decrease, and so forth. Note that for the loads presented here, the plastic region is never reached more than once.

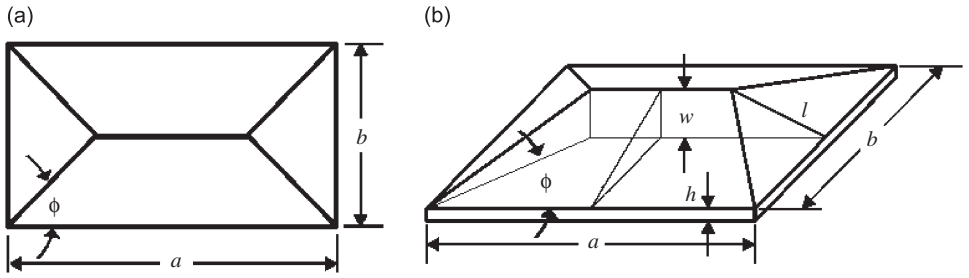

Fig. 2. Rooftop geometry of plastic deformation: (a) plan view, (b) isometric view.

4. Plastic response model

The plastic model used is Jones' hinge line method [21,22]. This method assumes a plastic deformation in the shape of a rooftop, shown in Fig. 2, with all the energy of the system dissipating through the hinge lines. Assuming that the in-plane displacements, velocities and accelerations are negligible, as well as assuming the geometry of deformation, an energy relationship between the external and inertial work rates and the internal energy dissipation is established. Assuming the angle $\phi = 45^\circ$, as per Nurick et al. [23], the final equation given in Florek and Benaroya [15] for the plastic model of a clamped plate is

$$\frac{\rho b^2}{\sigma_0 h}\left(\frac{2a}{b}-1\right)\ddot{w}+\frac{24a}{b}\frac{w}{h}+8\frac{h}{w}=\frac{Pb^2}{\sigma_0 h^2}\left(\frac{3a}{b}-1\right). \tag{16}$$

Solving for w results in the maximum transverse deflection of the clamped, rectangular plate.

4.1. Failure criteria

To determine whether the plate fails due to the blast load, the maximum allowable transverse deflection for the aluminum plate is calculated. This is done using the rupture strain value of 18% for aluminum 2024-T3 [24]. Since the deflection of the plate within the plastic region is the rooftop shape shown in Fig. 2, the smaller side of the rectangular plate, b, will be the limiting factor for failure. Making sure line l in Fig. 2 does not elongate 18% of its original length, the maximum possible transverse deflection before failure is calculated. The plate properties used for all cases in this study are shown in Table 1. These dimensions and properties of the plate represent the aluminum skin of a commercial aircraft's midsection between its frames and stringers. Using these dimensions the failure deflection, maximum allowable value of w, is approximately 63.6 mm. If the deflection reaches this value the plate is considered to fail.

5. Loading model

For a blast load, chemical investigation and experimental data [1–3,8,9] show that a good representative simplified model is an exponential time history. One of the most frequently used blast model is an exponential decay model with an initial peak pressure governed by the modified Friedlander equation,

$$P(t)=\begin{cases}0, & 0\leqslant t\leqslant T_a,\\ P_{\max}\left(1-\dfrac{t}{T_{\mathrm{dur}}}\right)\mathrm{e}^{-\alpha(t/T_{\mathrm{dur}})}, & T_a\leqslant t\leqslant T_{\mathrm{dur}},\\ 0, & T_{\mathrm{dur}}\leqslant t,\end{cases} \tag{17}$$

where $P(t)$ is the overpressure at time t, $P_{\max}$ is the maximum overpressure, T_a is the arrival time from detonation point to the object, T_{dur} is the overpressure duration time and α is the exponential decay constant. Fig. 3 is a graphical representation of this simplified loading model, where P_0 is the ambient pressure. The modified Friedlander equation neglects any negative overpressure phase of a blast load. The negative overpressure phase is that below ambient pressure that sometimes occurs at the tail end of a blast load. As

Table 1
Plate properties.

a	508 mm (20.0 in)
b	203 mm (8.00 in)
h	1.60 mm (0.0630 in)
ρ	2780 kg/m^3
E	7.31 GPa
v	0.330
σ_0	345 GPa

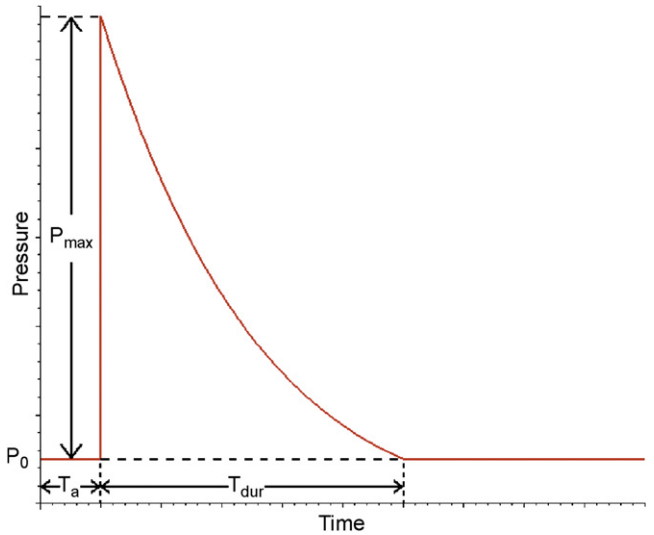

Fig. 3. Simplified blast loading model representative of the modified Friedlander equation, where the negative overpressure phase after time T_{dur} has been cutoff.

Gantes and Pnevmatikos [11] mention, this pressure phase is less significant as α is larger than one. In this study we chose loading profiles which satisfy this criterion. We also assume the explosive is far enough away from the object that we can approximate the loading as a planar blast wave over the entire object. In addition, since the arrival time does not affect the response of the plate in this study, the arrival time is set to zero.

Two types of simplified blast loading models are considered, as shown in Figs. 4a and b. Load 1 is the common modified Friedlander model described previously and Load 2 is the same except for the linear rise rather than the instantaneous rise. Load 2 is governed by

$$P(t) = \begin{cases} (P_{\max}/T_{\max})t, & 0 \leqslant t \leqslant T_{\max}, \\ P_{\max}\left(1 - \dfrac{t - T_{\max}}{T_{\text{dur}}}\right) e^{-\alpha(t-T_{\max})/T_{\text{dur}}}, & T_{\max} \leqslant t \leqslant T_{\text{dur}}, \\ 0, & T_{\text{dur}} \leqslant t, \end{cases} \tag{18}$$

where the rise time, $T_{\max}$, is the time at which the maximum pressure occurs.

5.1. Obtaining parameter values

Using the Hopkinson–Cranz blast scaling law, the values of $P_{\max}$, T_{dur} and α, are characterized by the scaled distance, Z,

$$Z = \frac{R}{M^{1/3}}, \tag{19}$$

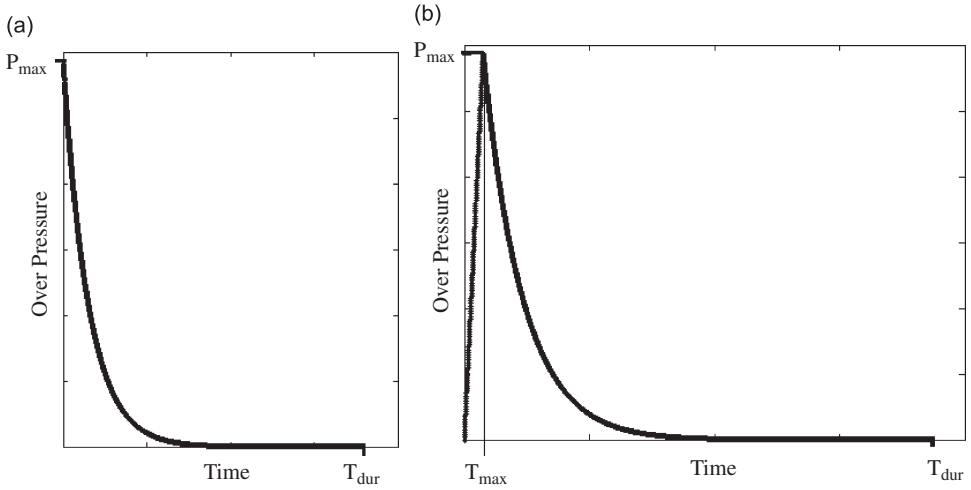

Fig. 4. (a) Load 1. Instantaneous rise with an exponential decay. (b) Load 2. Linear rise with an exponential decay.

where R is the standoff distance between the spherical charge center and the plate in meters, and M is the charge mass, which is expressed in kilograms of equivalent TNT. Two blast loads are considered to have the same loading profile if they have the same Z value. The smaller the Z value, the stronger the blast load.

Using the program ConWep [25], it is possible to generate the loading parameter values for various air blasts. This computer simulation uses values gathered through experiments given in the government manual TM 5-855-1, which makes use of Kingery and Bulmash [7]. According to Esparza [8], Kingery and Bulmash supply polynomial curve fits from values found in various literature [26–30]. For appropriate Z values, ConWep provides values for the normally reflected overpressure, which is used for $P_{\max}$, and the positive phase duration, which is used for T_{dur} of the exponential decay.

ConWep does not provide the decay constant for the reflected pressure. Therefore, it needs to be calculated using the reflected impulse, I_r, which ConWep does provide. Knowing that

$$I_r = \int_0^{T_{\mathrm{dur}}} P(t)\,\mathrm{d}t, \tag{20}$$

where P is the overpressure given by Eq. (17), one can find that

$$\frac{P_{\max} T_{\mathrm{dur}} \mathrm{e}^{-\alpha}(\alpha \mathrm{e}^{\alpha} - \mathrm{e}^{\alpha} + 1)}{\alpha^2} - I_r = 0. \tag{21}$$

Substituting the ConWep values of $P_{\max}$, T_{dur} and I_r into Eq. (21) allows one to find the decay constant, α, numerically.

Since there is no widely used loading model representative of Load 2, there is no convention or table of values to calculate $T_{\max}$. Experimental pressure loads [9,31] show the rise time to be very short. In the scaling of milliseconds, the rise times seem to be nearly instantaneous in many experiments. Depending on the instrumentation, experimental setup and explosive used the rise times may be difficult to obtain accurately. In addition, the larger the load, the faster the rise time. Typical values for rise times can vary from a few microseconds to milliseconds depending on the explosive used, the amount used and the distance to the target. We decided to estimate $T_{\max}$ as a percentage of the blast's arrival time because the arrival time is representative of its speed and initial distance to the object and contains the trend just mentioned. By examining a few cases and designing Loads 1 and 2 to have some differences in shape, it was determined that the rise time, $T_{\max}$, would be set equal to 10% of the arrival time, which can be obtained through ConWep. In addition, in order for the exponential decay of Load 2 to have the same shape as Load 1, the value of $T_{\max}$ must be added to the value of T_{dur} of Load 1 to obtain the value of T_{dur} for Load 2.

5.2. Six cases

Three values of the scaled distance Z are used: $Z = 0.7$, 1.2 and 2.0. The values obtained for the loading parameters of Loads 1 and 2 for each Z case studied here are shown in Tables 2 and 3, respectively. Figs. 5 and 6 show the first 0.8 ms of the loading profiles for each Z value of Loads 1 and 2, respectively.

6. Parameter sensitivities

Before randomizing the various loading parameters to determine their sensitivity, we first must determine the deterministic responses and maximum deflections. Using a fourth-order Runge–Kutta method, as described by Jaluria [32], the response is deterministically solved for each of the six loading cases. Fig. 7 shows the deterministic responses for Cases 2 and 5. The deflections are elastic from 0 to 0.127 ms and from 0 to 0.150 ms for Cases 2 and 5, respectively. From 0.127 to 0.336 ms and from 0.150 to 0.377 ms the responses are plastic for Cases 2 and 5, respectively. After 0.336 ms and 0.377 ms, for Cases 2 and 5, respectively, the responses decrease elastically and continue to be modeled elastically since the deflection never surpasses the previous maximum deflection. Table 4 lists the maximum deflections of the plate for each case. As expected, the maximum deflections of the plate are larger for the cases with smaller Z values. In addition, for a particular Z value, Load 2 produces a larger maximum deflection than Load 1. This is due to the extra impulse from under the linear-rise region of Load 2. The smallest Z value of 0.7 was chosen so that the maximum deflection from the deterministic run was just under the allowable maximum deflection before plate failure.

After the deterministic solutions have been calculated, one of the loading parameters is assumed random while leaving the remaining variables deterministic. The ensemble average of the response is evaluated using a Monte Carlo scheme as described by Benaroya and Han [33]. This procedure is repeated for each loading parameter and case. By comparing the maximum deflections of the random runs to the deterministic run for each loading case, the sensitivity of each loading parameter is calculated per case. A random parameter is considered more sensitive to uncertainty if the difference of maximum deflections of the plate between the deterministic and probabilistic models is greater.

6.1. Probability distribution

Since blast loads are so complex that they may be modeled as random, and there is little information on the different loading parameters' randomness, all the random variables are assumed to have uniform probability

Table 2
Loading parameter values of the three Z cases for Load 1.

	Loading parameter	Case 1 $Z = 0.70$	Case 2 $Z = 1.2$	Case 3 $Z = 2.0$
P_{max}	Maximum pressure	13.40 MPa	2.900 MPa	0.6458 MPa
T_{dur}	Duration time	0.8346 ms	1.792 ms	1.846 ms
α	Decay constant	11.296	10.784	3.7365

Table 3
Loading parameter values of the three Z cases for Load 2.

	Loading parameter	Case 4 $Z = 0.70$	Case 5 $Z = 1.2$	Case 6 $Z = 2.0$
P_{max}	Maximum pressure	13.40 MPa	2.900 MPa	0.6458 MPa
T_{dur}	Duration time	0.8622 ms	1.867 ms	2.040 ms
α	Decay constant	11.296	10.784	3.7365
T_{max}	Rise time	0.02765 ms	0.0750 ms	0.1944 ms

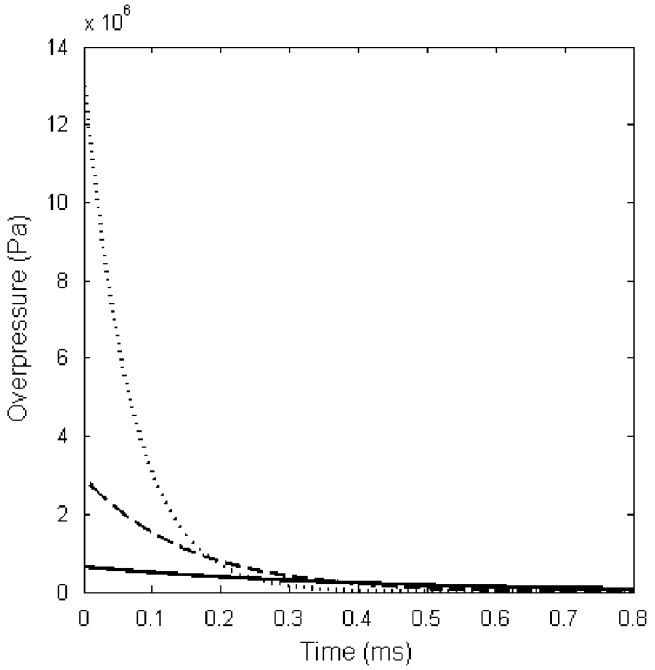

Fig. 5. Loading profiles of Load 1 with $Z = 0.7$ (...), $Z = 1.2$ (—) and $Z = 2.0$ (- - -). Although the duration times for each case are greater, only the first 0.8 ms are shown in this figure. Also note, in this scaling due to the larger overpressure of the $Z = 0.7$ case, the appearance of the larger Z value cases begin to lose their exponential decay shape.

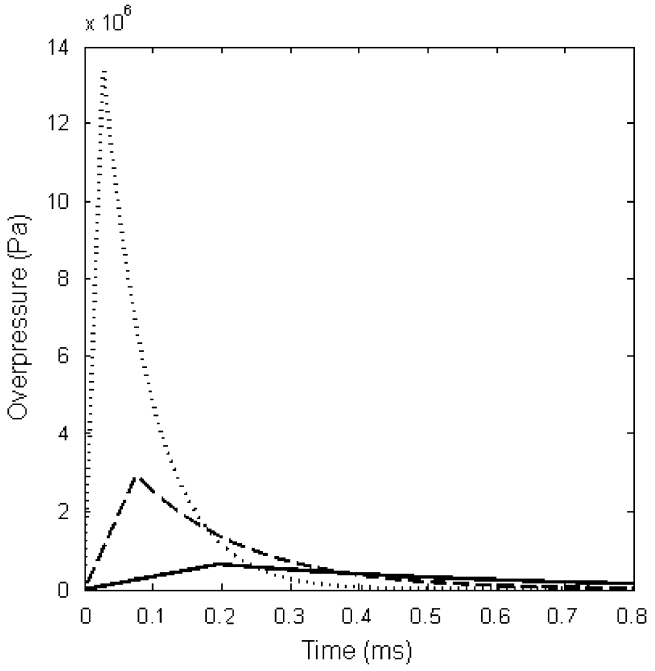

Fig. 6. Loading profiles of Load 2 with $Z = 0.7$ (...), $Z = 1.2$ (—) and $Z = 2.0$ (- - -). Although the duration times for each case are greater, only the first 0.8 ms are shown in this figure. Also note, in this scaling due to the larger overpressure of the $Z = 0.7$ case, the appearance of the larger Z value cases begin to lose their exponential decay shape.

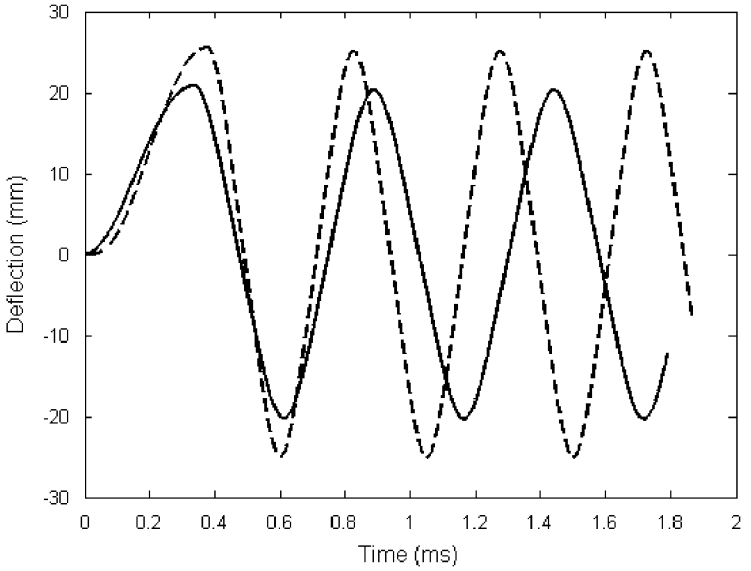

Fig. 7. Deterministic defections for Cases 2 (—) and 5 (- - -). The deflections are elastic from 0 to 0.127 ms and from 0 to 0.150 ms for Cases 2 and 5, respectively. From 0.127 to 0.336 ms and from 0.150 to 0.377 ms the responses are plastic for Cases 2 and 5, respectively. After 0.336 and 0.377 ms, for Cases 2 and 5, respectively, the responses decrease elastically and continue to be modeled elastically since the deflection never surpasses the previous maximum deflection.

Table 4
Maximum deflections of deterministic solution.

Case	Max. defection (mm)
1	48.1813
2	20.8533
3	10.1719
4	58.9217
5	25.5814
6	11.4930

density. In addition, using a uniform density makes it easier to specify a range of values for each random variable. In this paper, the term half-range (HR) is used to define the range between the mean value and the upper or lower values of the parameter. This is half of the total range in a uniform distribution. For a uniform density, the standard deviation σ is related to the half-range by the relation

$$\sigma = \frac{\mathrm{HR}}{\sqrt{3}}. \tag{22}$$

See Fig. 8. Each random variable's half-range is given as a percentage of its mean value. This also allows for a direct comparison between the various random parameters.

The deterministic parameter values shown in Tables 2 and 3 are taken to be the mean values. To obtain realizations for each parameter, a standard uniform number is generated and then transformed using

$$n(r) = \mu(r) + \mathrm{HR}(r) \times (2 \times \mathrm{rand} - 1), \tag{23}$$

where $n(r)$ is the realization for parameter r, $\mu(r)$ is the mean value and $\mathrm{HR}(r)$ is the half-range, where

$$\mathrm{HR}(r) = \mu(r) \times \mathrm{HR}_f \tag{24}$$

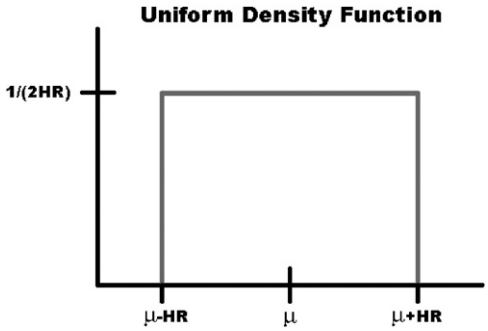

Fig. 8. Visual representation of half-range where μ is the mean and HR represents the half-range.

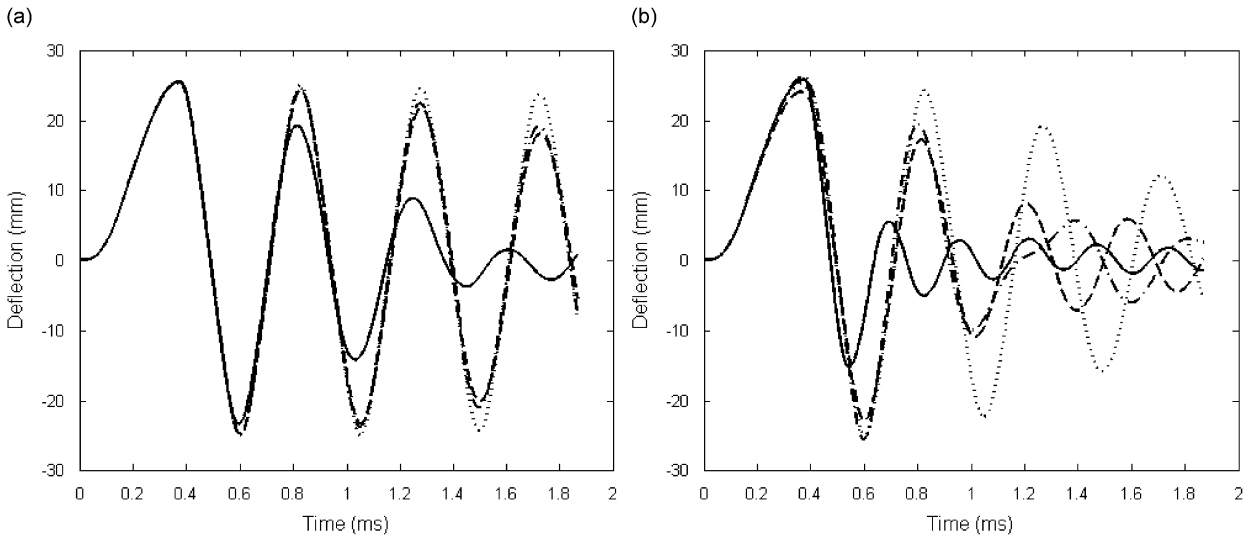

Fig. 9. In these figures, each deflection is for a simulation where P_{max} (—), T_{dur} (- - -), α (– · – · –) or T_{max} (. . .), is the random variable with (a) $HR_f = 0.2$ and (b) $HR_f = 0.8$ for Case 5. For example, the solid line deflection is for the simulation where P_{max} is the random variable.

and HR_f is the half-range factor. The half-range factor is a number between 0 and 1 that determines the level of uncertainty for the random parameter. The closer the half-range factor is to 1 the higher the level of uncertainty. The function rand is an internal MATLAB function that generates a uniformly distributed random number between 0 to 1. For each random variable run, the seed for the rand command in MATLAB is reset. This ensures that the same sequence of random numbers are generated for each run.

6.2. Averaging response

The average response in the Monte Carlo method must be calculated at every time step since the loading and response of the plate are time dependent. This procedure is known as ensemble averaging. Only the runs for which the plate does not fail are factored into the averaged response since response Eqs. (12) and (16) are not valid when the plate fails. The time stepping value for the program is set at 0.5 μs. This is a very small time step, even for blast loads, but this value allows for accurate tracking.

For all the following results, the labeled variable is the loading model parameter that is the random variable for that particular result. Figs. 9a and b are time histories of the average deflections produced for each random variable of Case 5 when $HR_f = 0.2$ and 0.8, respectively. These time histories tend to decay more rapidly as

the uncertainty is increased. In addition, the deflection shape sensitivity is greatest when $P_{\max}$ is the random variable.

Figs. 10a–d show the responses for select cases when $\mathrm{HR}_f = 0.8$. For all cases, the maximum deflection occurs at the first local maximum. Thus, the deflections reach the plastic region only once for all cases.

Tables 5–10 show results with various HR_f for Cases 1–6, respectively. The random variable All represents runs where all of the loading parameters are random. For each random variable and case, the difference in maximum deflection, Δ, is calculated using

$$\Delta = det_{\max} - prob_{\max}, \tag{25}$$

where $det_{\max}$ is the maximum deflection of the deterministic model and $prob_{\max}$ is the maximum deflection of the averaged response for the probabilistic model. In addition to Δ, the percent error of the maximum deflection, % Error, is calculated by

$$\%\mathrm{Error} = \frac{|\Delta|}{det_{\max}} \times 100. \tag{26}$$

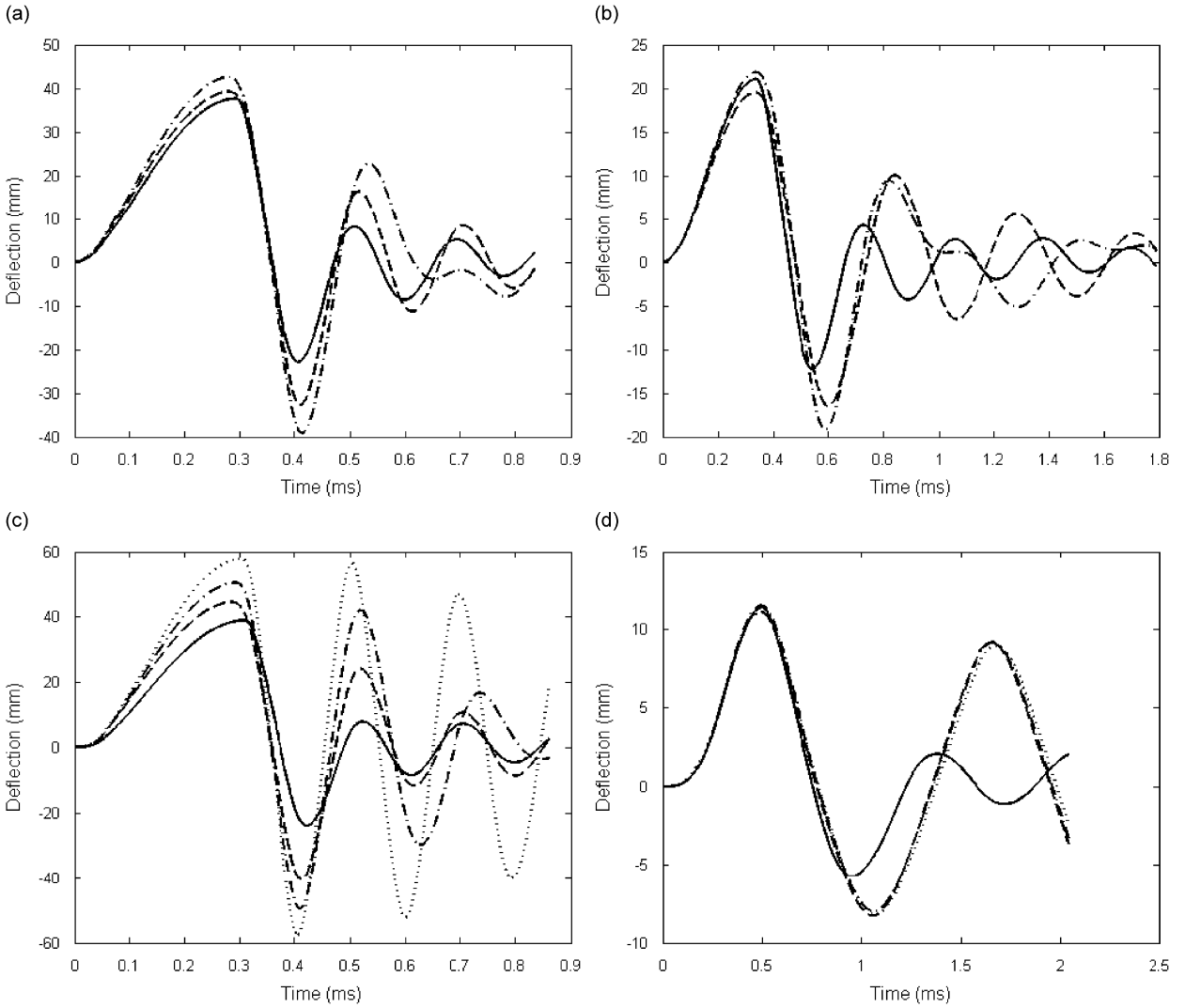

Fig. 10. Average deflections with $\mathrm{HR}_f = 0.8$ for (a) Case 1, (b) Case 2, (c) Case 4 and (d) Case 6 where $P_{\max}$ (—), T_{dur} (- - -), α (– · – · –) or $T_{\max}$ (. . .), is the random variable. The maximum deflection of the response for all cases occurs at the first local maximum.

Table 5
Case 1 differences, percent errors and probability of plate failures.

Random variable	Δ (mm)	% Error	Prob. of failure
Half-range = 10% of the mean ($HR_f = 0.1$)			
P_{max}	−0.0221	0.0458	0
T_{dur}	−0.2383	0.4945	0
α	0.0057	0.0118	0
All	−0.1333	0.2766	0
Half-range = 40% of the mean ($HR_f = 0.4$)			
P_{max}	−1.4066	2.9194	0.0821
T_{dur}	−0.9560	1.9841	0
α	−0.2262	0.4694	0.0812
All	−5.5229	11.4627	0.1833
Half-range = 80% of the mean ($HR_f = 0.8$)			
P_{max}	−10.5214	21.8371	0.2906
T_{dur}	−8.9209	18.5152	0.2215
α	−5.5163	11.4491	0.2929
All	−17.0795	35.4485	0.3017

Table 6
Case 2 differences, percent errors and probability of plate failures.

Random variable	Δ (mm)	% Error	Prob. of failure
Half-range = 80% of the mean ($HR_f = 0.8$)			
P_{max}	0.2165	1.0381	0
T_{dur}	−1.3229	6.3436	0
α	1.0026	4.8079	0
All	−0.3126	1.4989	0

Table 7
Case 3 differences, percent errors and probability of plate failures.

Random variable	Δ (mm)	% Error	Prob. of failure
Half-range = 80% of the mean ($HR_f = 0.8$)			
P_{max}	−0.2628	2.5833	0
T_{dur}	−0.5073	4.9874	0
α	0.0682	0.6707	0
All	−0.7307	7.1836	0

The probability of plate failure is also given for each probabilistic run. The percent errors are a measure of how much sensitivity the parameters have to uncertainty. The larger percent error a random variable produces, the greater that parameter's sensitivity is to uncertainty. Note, the percent errors are calculated using the maximum deflections of the averaged responses, which do not include any of the runs with plate failures. As expected, these percent errors increase as the uncertainty, or HR_f value, increases. For a given case, as HR_f increases the random variables' sensitivity to uncertainty (i.e., percent errors) maintain the same sequence when ordered from greatest to least. For instance, looking at Case 1, Table 5, the order of random variables from greatest to least percent error when $HR_f = 0.8$ is All, P_{max}, T_{dur} and then α. One can see that this is the same order when $HR_f = 0.4$ for Case 1. This is always true except when the percent errors are very small.

For Cases 2, 3 and 5, the duration time, T_{dur}, is the most sensitive parameter due to uncertainty since the greatest percent error for those cases occurs when T_{dur} is the random variable. In addition, for Cases 2 and 5,

Table 8
Case 4 differences, percent errors and probability of plate failures.

Random variable	Δ (mm)	% Error	Prob. of failure
Half-range = 10% of the mean ($HR_f = 0.1$)			
P_{max}	−0.4683	0.7948	0.0841
T_{dur}	−0.2236	0.3795	0
α	0.0134	0.0227	0
T_{max}	0.003	0.0051	0
All	−1.2499	2.1213	0.1493
Half-range = 40% of the mean ($HR_f = 0.4$)			
P_{max}	−8.9262	15.1493	0.3993
T_{dur}	−5.8432	9.9169	0.3318
α	−4.051	6.8753	0.3431
T_{max}	−0.038	0.0645	0
All	−11.3514	19.2652	0.3838
Half-range = 80% of the mean ($HR_f = 0.8$)			
P_{max}	−20.2262	34.3273	0.4518
T_{dur}	−14.5803	24.7452	0.4095
α	−8.6061	14.6061	0.4209
T_{max}	−1.2879	2.1858	0.1678
All	−24.3052	41.2500	0.4057

Table 9
Case 5 differences, percent errors and probability of plate failures.

Random variable	Δ (mm)	% Error	Prob. of failure
Half-range = 10% of the mean ($HR_f = 0.1$)			
P_{max}	0.0424	0.1657	0
T_{dur}	−0.0452	0.1767	0
α	0.0444	0.1736	0
T_{max}	0.0061	0.0238	0
All	0.0186	0.0726	0
Half-range = 40% of the mean ($HR_f = 0.4$)			
P_{max}	0.0553	0.2161	0
T_{dur}	−0.4719	1.8448	0
α	0.1209	0.4728	0
T_{max}	−0.0657	0.2568	0
All	−0.2885	1.1276	0
Half-range = 80% of the mean ($HR_f = 0.8$)			
P_{max}	0.2588	1.0117	0
T_{dur}	−1.5168	5.9294	0
α	0.6462	2.5261	0
T_{max}	−0.3630	1.4191	0
All	−1.1466	4.4823	0

parameter T_{dur} is more sensitive to uncertainty than when all the parameters are assumed random at the same time. This is due to the fact that when parameter α is the random variable, the averaged response tends to have an increase in its maximum deflection as the random variable's uncertainty increases. In contrast, when the other parameters are assumed random, the averaged responses tend to have a decrease in the maximum deflection as the random variables' uncertainties increase. For Case 6, the most sensitive parameter due to uncertainty is the rise time, T_{max}. The reason for random variable T_{max} to have the highest sensitivity to uncertainty for this case is because the mean value of T_{max} is an order of magnitude greater in Case 6 than the

Table 10
Case 6 differences, percent errors and probability of plate failures.

Random variable	Δ (mm)	% Error	Prob. of failure
Half-range = 80% of the mean ($HR_f = 0.8$)			
P_{max}	−0.0928	0.8076	0
T_{dur}	−0.3679	3.2012	0
α	0.0141	0.1223	0
T_{max}	−0.4002	3.4817	0
All	−0.8675	7.5483	0

other cases, making the linear rise part of the forcing function the main contributor to the load. However, the sensitivity of parameter T_{dur} is very close to parameter T_{max}'s sensitivity to uncertainty.

Only Cases 1 and 4 have results with probability of plate failures greater than zero. As seen in Tables 5 and 8, the probability of plate failures increase as the uncertainty increases. With a higher probability of plate failure, a greater number of runs with high deflections are not included in the averaged response. This means that the more plate failures there are, the lower the averaged response tends to be compared to the deterministic deflection. This yields to a greater percent error.

At low levels of uncertainty for Case 1, where there are no plate failures, T_{dur} is the most sensitive parameter due to uncertainty. However, as the uncertainty increases and the probability of plate failures increase, P_{max} becomes the most sensitive parameter due to uncertainty for Case 1. When all the parameters are random, the probability of plate failure for Case 1 is the greatest at 30.17%. When α and P_{max} are random the probability of plate failures are 29.29% and 29.06%, respectively.

For Case 4, P_{max} is the most sensitive parameter due to uncertainty. Random variable P_{max} also produces the greatest probability of plate failure as uncertainty increases. In fact, when $HR_f = 0.8$, random variables P_{max} and T_{dur} produce a greater probability of plate failure than when all the parameters are random at the same time.

6.3. Standard deviations

The standard deviation for each time step is calculated by

$$\sigma(t) = \sqrt{\frac{\sum_{i=1}^{N}(w_i(t) - w_{ave}(t))^2}{N}}, \tag{27}$$

where $\sigma(t)$ is the standard deviation at time t, $w_i(t)$ is the response of run i at time t, N is the number of runs that do not have plate failures and $w_{ave}(t)$ is the averaged response. This standard deviation is a measure of the spread, or scatter, of the response values. The standard deviation is also useful for creating confidence bounds. Figs. 11a and b depict the deflections with random variable T_{dur} along with one standard deviation bounds for Case 2 when $HR_f = 0.2$ and 0.8, respectively. As expected, as the uncertainty increases, the standard deviation of the response increases.

In addition to the time dependent standard deviation described by Eq. (27), the standard deviation of the maxima of each run is also calculated. For this standard deviation there is no time dependence and the maxima of each run are taken regardless of when they occur. The equation is

$$\sigma_{max} = \sqrt{\frac{\sum_{i=1}^{N}(w_{max_i} - w_{ave_{max}})^2}{N}}, \tag{28}$$

where σ_{max} is the standard deviation of the maxima, w_{max_i} is the maximum value of run i, N is the number of runs that do not have plate failures and $w_{ave_{max}}$ is the maximum of the averaged response. These standard deviations of maximum values increase as the half-range increase. This is what would be expected since a higher half-range implies a more random and scattered result. Table 11 shows the results for all the cases and

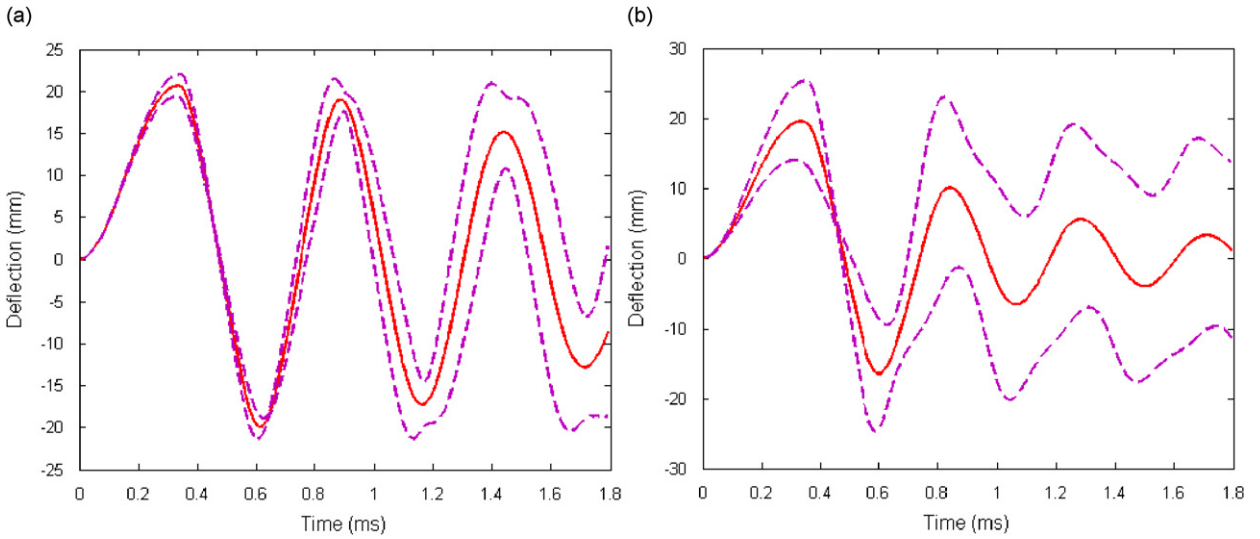

Fig. 11. Deflection (–) and one standard deviation bounds (- - -) for Case 2 for random variable T_{dur} and (a) $HR_f = 0.2$ and (b) $HR_f = 0.8$.

Table 11
Standard deviation of maximum values when $HR_f = 0.8$.

$HR_f = 0.8$	P_{max} (mm)	T_{dur} (mm)	α (mm)	T_{max} (mm)	All (mm)
Case 1	15.17	14.82	9.27	N/A	15.63
Case 2	8.16	5.68	5.65	N/A	11.77
Case 3	2.52	1.35	0.84	N/A	3.01
Case 4	14.56	11.67	6.25	3.52	14.71
Case 5	10.39	5.03	4.80	1.83	12.69
Case 6	3.13	0.85	0.49	0.36	3.11

variables when $HR_f = 0.8$. For most cases, the largest standard deviation occurs when all the variables are random. For the individual parameters, the order of standard deviations from greatest to least is P_{max}, T_{dur}, α and then T_{max}.

7. Trends of maximum deflection as uncertainty increases

In order to see the trends of the plate's maximum deflection as the uncertainty of each parameter increases, the averaged response was calculated 100 times per random variable, with random half-ranges from 0% to 80% of the random variable's mean. The maximum deflection of each averaged response is then plotted against a normalized half-range, defined as the half-range value divided by 80% of the random variable's mean. This allows for a direct comparison between the various loading parameters' trends. Fig. 12 shows the results for Case 5. For Cases 2 and 5, as the uncertainty in parameter P_{max} increases, the maximum deflection of the plate tends to be constant but with a larger scatter. For all the other cases, the maximum deflection of the plate tends to decrease as parameter P_{max}'s uncertainty increases. For all six cases, the plate's maximum deflection tends to decrease as the uncertainty increases in parameters T_{max}, T_{dur} and when all of the parameters are random. For the cases with no plate failures (Cases 2, 3, 5 and 6) the plate's maximum deflection tends to increase as the uncertainty of parameter α increases.

Fig. 13a shows the maximum deflection trends of each parameter for Case 4. This plot shows a decreasing maximum deflection trend for all the parameters, which is also true for Case 1. However, as mentioned before,

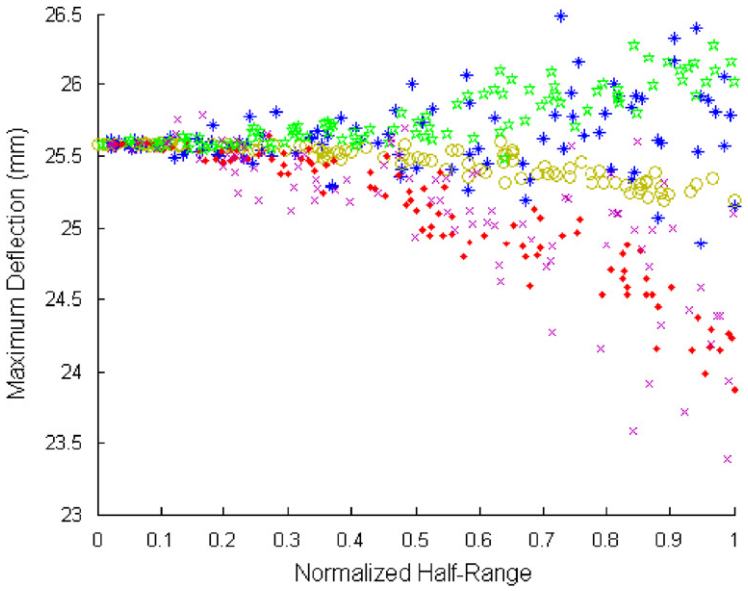

Fig. 12. Scatter plot of maximum deflections vs. normalized half-range for Case 5 where P_{max} (*), T_{dur} (·), α (⋆), T_{max} (○), or All (×) is the random variable.

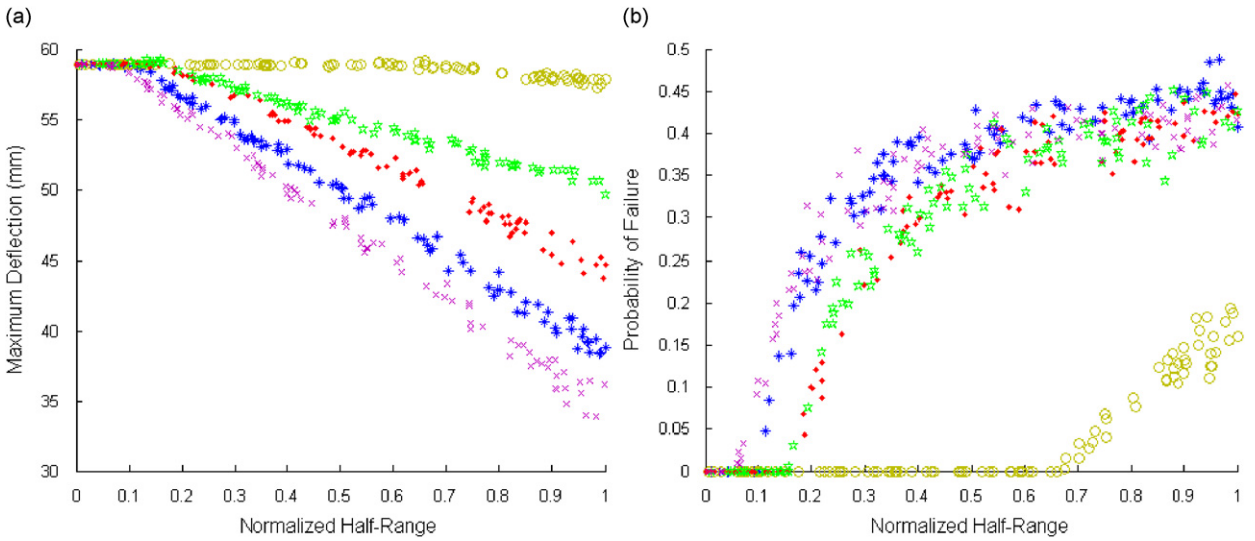

Fig. 13. (a) Scatter plot of maximum deflections vs. normalized half-range for Case 4 where P_{max} (*), T_{dur} (·), α (⋆), T_{max} (○), or All (×) is the random variable. (b) Probability of failure vs. normalized half-range for Case 4 where P_{max} (*), T_{dur} (·), α (⋆), T_{max} (○), or All (×) is the random variable.

this is due to the fact that the runs with plate failures, which have a high deflection, are not included in the averaged response. For Cases 1 and 4, the maximum deflection decreases the most with increasing uncertainty when all of the parameters are random. For the individual random parameters, the maximum deflection when P_{max} is the random variable decreases the most with increasing uncertainty. This decreasing maximum deflection trend is highly related to the probability of failure for each parameter.

Fig. 13b shows the probability of plate failure as uncertainty increases for each parameter of Case 4. Each random parameter initially shows a zero probability of plate failure and then at a certain level of uncertainty, the probability of plate failure begins to increase as the uncertainty increases. For both Cases 1 and 4, as uncertainty increases, plate failures are first observed when all the parameters are random. For Case 1, for

random variables P_{max} and α, plate failures begin to occur around the same level of uncertainty at a normalized half-range of about 0.42. For random variable T_{dur} the plate failures do not start to occur until a higher level of uncertainty, which is at a normalized half-range of 0.55. For the individual parameters of Case 4, when P_{max} is the random variable the response begins to show plate failures first, which is at a normalized half-range of 0.1. For random variables T_{dur} and α, plate failures begin to occur around the same level of uncertainty, which is at a normalized half-range of about 0.17. For Case 4, random variable T_{max} results in the smallest probability of plate failure and a zero probability of plate failure until a normalized half-range of about 0.68, which is a larger level of uncertainty compared to the other parameters. By observing Figs. 13a and b, it can be seen that as each probability of plate failure begins to increase, the corresponding maximum deflection of the plate begins to decrease.

8. Probability densities for maximum deflection

The probability density functions of the plate's maximum deflections for Case 5 when $HR_f = 0.8$ are presented in Figs. 14a–d. Although only Case 5 is shown here, the other cases have similar shapes for each

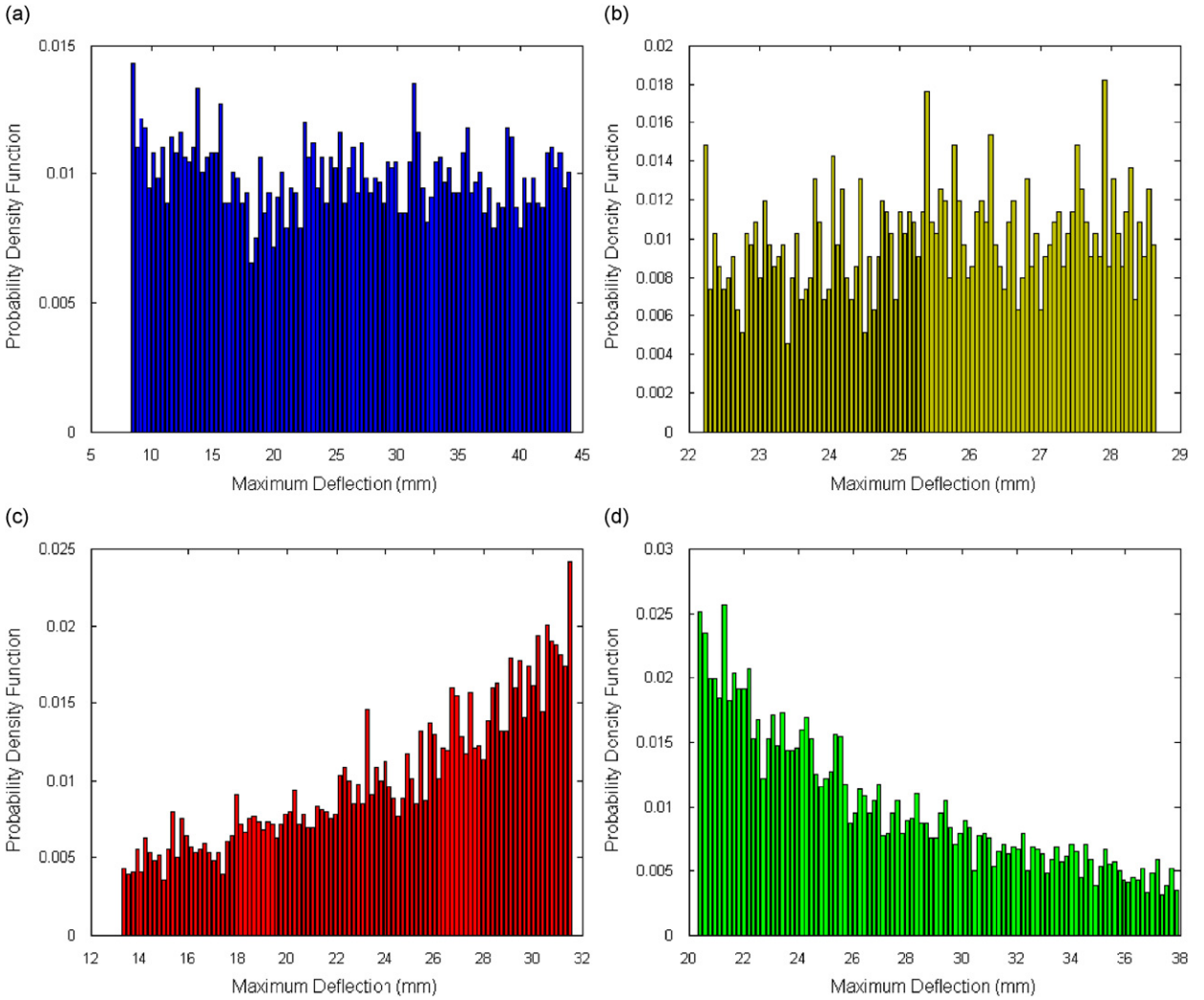

Fig. 14. Probability density of maximum deflection in Case 5 with $HR_f = 0.8$ for random parameters: (a) P_{max} using 5173 simulation runs, (b) T_{max} using 1756 simulation runs, (c) T_{dur} using 5622 simulation runs and (d) α using 5451 simulation runs.

random parameter. The probability density functions due to random parameters P_{max} and T_{max}, shown in Figs. 14a and b, respectively, have a uniform distribution. However, as Fig. 14c shows, random variable T_{dur} leads to a probability density function that has more area under larger maximum deflections. This means there is a greater probability of obtaining higher maximum deflections when T_{dur} is the random variable. Conversely, Fig. 14d shows the probability density function due to random variable α has more area under the smaller maximum deflections, giving a greater probability to obtain lower deflections. These figures are very useful to show the range of the plate's maximum deflections given a particular random variable. In addition, they can be used to generate confidence bounds.

9. Using deterministic results to explain probabilistic results

To understand why these probability density functions are shaped this way, as well as to explain the trends of the maximum deflection as uncertainty increases, the deterministic, maximum deflection for each parameter is calculated for all the values within the full range of minus to plus 80% of that variable's mean. Figs. 15a–d

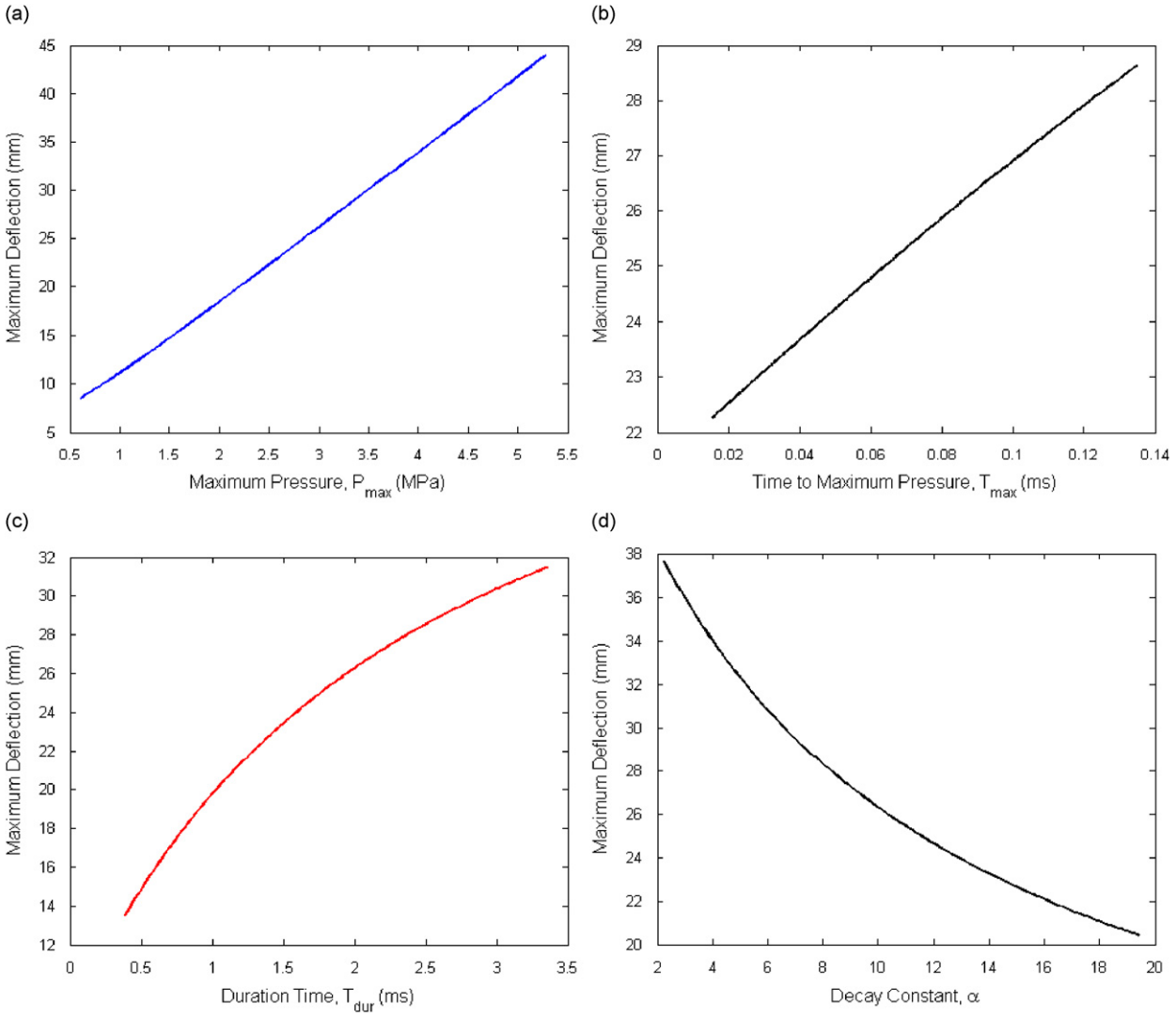

Fig. 15. Deterministic results for maximum deflection in Case 5 for parameters: (a) P_{max}, (b) T_{max}, (c) T_{dur} and (d) α. The range for each parameter is its full range when $HR_f = 0.8$.

show these results for Case 5. For parameters P_{max} and T_{max} the maximum deflection of the response increases in a linear way as the parameter values increase. Due to this relationship, if a uniform distribution of the parameter is taken around the mean value, the response will also have a uniform distribution with a mean deflection equal to the deflection of the parameter's mean value. This also explains why random parameters P_{max} and T_{max} have a straight horizontal maximum deflection trend for Case 5, because their averages with a uniform distribution, or any distribution that is symmetric about its mean value, will be the deflection at the mean value.

For parameter T_{dur}, shown in Fig. 15c, the maximum deflection increases with a concave down curve as the parameter values increase. Since the curve is concave down, the average maximum deflection of two points equidistant and on opposite sides of the mean will be less than the maximum deflection at the mean value, as seen in Fig. 16. This explains why the maximum deflection trends of random parameter T_{dur} are decreasing as its uncertainty increases. In addition, since the slope of the maximum deflection curve decreases as a function of T_{dur}, when one takes values within a fixed range, there will be a greater spread of maximum deflections at the lower values of T_{dur} than at the higher values. Also, since the maximum deflections are closer together in the higher values of T_{dur} than at the lower T_{dur} values for a fixed range, the probability of the maximum deflections at the higher T_{dur} range are greater. Thus, the probability density function is increasing as shown in Fig. 14c.

For parameter α, shown in Fig. 15d, the maximum deflection of the response decreases as a function of α. Since the curve is concave up, the average of the maximum deflections with a uniform distribution will be greater than the maximum deflection at the mean value, which explains why the maximum deflection trend for parameter α is increasing as its uncertainty increases. Fig. 15d shows the slope of the maximum deflection curve increases as a function of α. Thus the probability density function for random parameter α is decreasing as shown in Fig. 14d.

10. Summary of key results and conclusion

A random variable analysis of simplified blast loading model parameters is conducted to determine their sensitivity to uncertainty. In addition, some probabilistic analyses and observations of trends are performed as the uncertainties of the parameters increase. Six different loading cases, listed in Tables 2 and 3, were analyzed in this work.

For Cases 2, 3 and 5, deflections are most sensitive to uncertainty in T_{dur}. For Cases 1 and 4, P_{max} becomes the most sensitive parameter to uncertainty once the plate begins to fail for some of the runs. However, for the lower levels of uncertainty, before the plate begins to fail for any of the runs, T_{dur} is the most sensitive parameter to uncertainty. The reason for this transition is because the runs with plate failures are not included in the averaged response. Due to the fact that the linear rise of Case 6 is the main contributor of the load, parameter T_{max} is the most sensitive to uncertainty, although parameter T_{dur}'s sensitivity to uncertainty

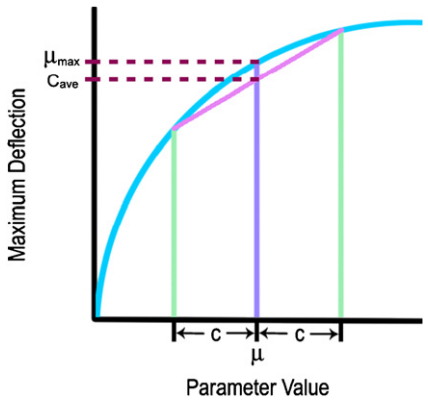

Fig. 16. Visual explanation for why the average value of a concave down plot with a fixed range will always be less than the value at the middle of that range.

(i.e., percent error) is almost the same. In addition, according to Esparza [8], T_{dur} is the most difficult of the parameters to measure, especially at small scaled distances. This means that in order to obtain a more accurate result, the measurement precision of T_{dur} needs to be improved upon more than those of the other parameters.

Besides determining which parameter is more sensitive to uncertainty, trends of the plate's maximum deflection due to the uncertainty level of loading parameters are examined. Uncertainty in parameter α tends to increase the maximum deflection of the plate, while the rest of the parameters' uncertainties tend to decrease it or keep it the same.

The maximum deflection probability density functions are created and show a uniform distribution for the parameters P_{max} and T_{max}, while the parameter T_{dur} has a distribution with positive slope and parameter α has a distribution with negative slope.

Finally, by examining deterministic plots of the plate's maximum deflection over the range of each parameter, many of the trends and features are able to be explained. This method can be applied to a wide range of problems.

The introduction of randomness in the key model parameters leads to significant differences in the mathematical predictions of the physical behavior of the system. Within that probabilistic description via the density function, the standard deviation—or measure of uncertainty—will determine the frequency of failure and the range of peak displacements. How the modeler selects these probabilistic parameters is important. Is the uncertainty due to a lack of knowledge about the process or due to the complexity and sensitivity of the process and thus its irreproducibility? Therefore, the predictions need to be examined in two parts. The first is related to the physical model and its applicability. The second is related to the probabilistic model and the degree to which it is knowledge-based.

Our mathematical model is a reduced-order model that is based on reasonable assumptions. Improvements are possible by relaxing assumptions, but at some point the mathematical difficulties outweigh the benefits of the reduced-order model and a larger scale computational model would make more sense. Our probabilistic model is non-presumptive, meaning that by using uniform densities for the parameters we are assuming that we only have confidence about the upper and lower bounds of the parameter values, and have no knowledge about their possible values within those bounds. As such, we can make relative physical conclusions on the system behavior, and how sensitive system behavior is to parameter probabilistic variations.

As we see from our results, such sensitivity is case dependent. Our view is that these results provide a guide to the experimentalist as well as to the analyst on the importance of particular data to the resulting behavior. These results suggest where the major efforts should be made for more accurate data.

Acknowledgments

The authors thank the Transportation Security Administration and Department of Homeland Security for their support of this research. In particular, we thank Howard Fleisher, Nelson Carey and Joseph Gatto of the Transportation Security Laboratory.

References

[1] G.F. Kinney, K.J. Graham, *Explosive Shocks in Air*, second ed., Springer, New York, NY, 1985.
[2] W.E. Baker, *Explosions in Air*, University of Texas Press, Austin, TX, 1973.
[3] W.E. Baker, P.A. Cox, P.S. Westine, J.J. Kulesz, R.A. Strehlow, *Explosions Hazards and Evaluation*, Elsevier Science Publishers B.V., Amsterdam, The Netherlands, 1983.
[4] J.R. Florek, H. Benaroya, Pulse-pressure loading effects on aviation and general engineering structures—review, *Journal of Sound and Vibration* 284 (2005) 421–453.
[5] F.B.A. Beshara, Modelling of blast loading on aboveground structures—I. General phenomenology and external blast, *Computers & Structures* 51 (1994) 585–596.
[6] J.M.K. Chock, R.K. Kapania, Review of two methods for calculating explosive air blast, *Shock and Vibration Digest* 33 (2001) 91–102.
[7] C.N. Kingery, G. Bulmash, Airblast parameters from TNT spherical air burst and hemispherical surface burst, Ballistic Research Laboratory Report No. ARBRL-TR-02555, Aberdeen Proving Ground, MD, 1984.

[8] E.D. Esparza, Blast measurements and equivalency for spherical charges at small scaled distances, *International Journal of Impact Engineering* 4 (1986) 23–40.
[9] J.A. Gatto, S. Krznaric, Pressure loading on a luggage container due to an internal explosion, in: Y.S. Shin, J.A. Zukas (Eds.), *Structures Under Extreme Loading Conditions-1996*, ASME, New York, NY, 1996, pp. 29–35.
[10] M.C. Simmons, G.K. Schleyer, Pulse pressure loading of aircraft structural panels, *Thin-Walled Structures* 44 (2006) 496–506.
[11] C.J. Gantes, N.G. Pnevmatikos, Elastic–plastic response spectra for exponential blast loading, *International Journal of Impact Engineering* 30 (2004) 323–343.
[12] Design of structures to resist the effects of accidental explosions, US Department of the Army Technical Manual, TM5-1300, Washington, DC, 1990.
[13] A.J. Watson, Loading from explosions and impact, in: A.J. Kappos (Ed.), *Dynamic Loading and Design of Structures*, Spon Press, London, New York, 2002, pp. 231–284.
[14] D. Bogosian, J. Ferritto, Y. Shi, Measuring uncertainty and conservatism in simplified blast models, *Presented at the 30th Explosives Safety Seminar*, Atlanta, GA, 2002.
[15] J.R. Florek, H. Benaroya, Simplified elastic–plastic modeling of thin, rectangular plates subjected to blast loading, *International Journal of Non-Linear Mechanics*, submitted for publication.
[16] H.F. Bauer, Nonlinear response of elastic plates to pulse excitations, *American Society of Mechanical Engineers Journal of Applied Mechanics* 35 (1968) 47–52.
[17] S.K. Singh, V.P. Singh, Mathematical modelling of damage to aircraft skin panels subjected to blast loading, *Defence Science Journal* 41 (1991) 305–316.
[18] J.R. Florek, Study of Simplified Models for the Large Deflection of Thin, Rectangular Plates Subjected to Blast Loading, Master's Thesis, Rutgers University, 2005.
[19] C. Massonnet, General theory of elasto-plastic membrane-plates, in: J. Heyman, F. Leckie (Eds.), *Engineering Plasticity: Papers for a Conference Held in Cambridge*, March 1968, Cambridge University Press, Cambridge, UK, 1968, pp. 443–471.
[20] J. Lee, Comparison of the two formulations of w-u-v and w-F in nonlinear plate analysis, *American Society of Mechanical Engineers Journal of Applied Mechanics* 69 (2002) 547–552.
[21] N. Jones, *Structural Impact*, Cambridge University Press, Cambridge, UK, 1989.
[22] N. Jones, T.O. Uran, S.A. Tekin, The dynamic plastic behavior of fully clamped rectangular plates, *International Journal of Solids and Structures* 6 (1970) 1499–1512.
[23] G.N. Nurick, H.T. Pearce, J.B. Martin, The deformation of thin plates subjected to impulsive loading, in: R.F.L. Bevilacqua, R. Valid (Eds.), *Inelastic Behaviour of Plates and Shells*, Springer, Berlin, 1986, pp. 597–616.
[24] ⟨www.matweb.com⟩.
[25] D.W. Hyde, ConWep: Conventional Weapons Effects Program, U.S. Army, Vicksburg, MS.
[26] H.J. Goodman, Compiled free air blast data on bare spherical Pentolite, Ballistic Research Laboratory Report No. 1092, Aberdeen Proving Ground, MD, 1960.
[27] C.N. Kingery, Air blast parameters versus distance for hemispherical TNT surface bursts, Ballistic Research Laboratory Report No. 1344, Aberdeen Proving Ground, MD, 1966.
[28] R. Reisler, B. Pellet, L. Kennedy, Air burst data from height-of-burst studies in Canada, Vol. II: HOB 45.4 to 144.5 feet, Ballistic Research Laboratory Report No. 1990, Aberdeen Proving Ground, MD, 1977.
[29] J.M.M. Swisdak, Explosion effects and properties: part I—explosion effects in air, Naval Surface Weapons Center Report No. NSWC/WOL/TR 75-116, White Oaks, Silver Spring, MD, October 1975.
[30] V.W. Davis, T. Goodale, K. Kaplan, A.R. Kriebel, H.B. Mason, J.F. Melichar, P.J. Morris, J.N. Zaccor, Nuclear weapons blast phenomena, Vol. IV—Simulation of Nuclear Airblast Phenomena with High Explosives (U), Defense Analytical Services Agency Report No. 1200-IV, Washington, DC, (SECRET - FRD), 1973.
[31] R.L. Veldman, J. Ari-Gur, C. Clum, A. DeYoung, J. Folkert, Effects of pre-pressurization on blast response of clamped aluminum plates, *International Journal of Impact Engineering* 32 (2006) 1678–1695.
[32] Y. Jaluria, *Computer Methods for Engineering*, Taylor and Francis, Washington, DC, 1996.
[33] H. Benaroya, S.M. Han, *Probability Models in Engineering and Science*, CRC Press, Boca Raton, FL, 2005.